DNS OF TRANSITIONAL BOUNDARY LAYER OVER COMPLIANT SURFACES

Wang Zhengyi[1], Yeo K. S.[2] and Khoo B. C.[2,3]
[1]Temasek Laboratories, National University of Singapore,
1 Engineering Drive 2, SINGAPORE 117576
[2]Department of Mechanical Engineering, National University of Singapore,
9 Engineering Drive 1, SINGAPORE 117576
[3]Singapore-MIT Alliance, National University of Singapore,
4 Engineering Drive 3, SINGAPORE 117576

Corresponding Author: Yeo K.S., e-mail: mpeyeoks@nus.edu.sg

ABSTRACT

In this work, the complex interaction of a boundary layer transition flow and the compliant surface is studied using the Spatial Direct Numerical Simulations (SDNS). This is carried out for 2D and 3D unsteady boundary layer flow over compliant surfaces.

Our 2D simulations demonstrated that the Compliant Induced Flow Instability (CIFI) waves could be induced by the presence of finite compliant walls. The coexistence of TS and CIFI wave has made it difficult to study the behavior of the individual waves. Nevertheless, results showed that well-designed compliant surface could reduce the amplification rate and cause the unstable region of TS waves. Computations for 3D linear waves over finite membranes showed that the 3D oblique TS and CIFI waves excited by the same frequency and same spanwise wavenumber disturbance generally propagated at different angles when they traveled downstream. Simulations of subharmonic breakdown over membrane revealed that compliant surfaces could in some instances lessen nonlinear interactions of instability waves in a transitional boundary layer.

INTRODUCTION

Linear and various nonlinear stability theories have demonstrated that even simple compliant surfaces, such as membrane/plate surfaces (Carpenter & Garrad 1985, 1986; Thomas 1992a, b) and homogeneous viscoelastic layers (Yeo 1986, 1988), can offer a certain transition-delay effects. There is one important limitation to these studies however, that is, they are essentially 'local' in character and could not take adequate account of global features such as the edge effects of finite panels. Moreover, researchers are beginning to turn their attention to more complex wall models (inhomogeneous walls and walls with varying properties) in order to obtain improved transition-delaying performance. Nevertheless, existing linear and nonlinear theoretical methods are difficult to be extended for investigating these complex wall models. The strong elliptic effect of wall dynamics and flow-wall interaction prevents the application of a semi-theoretical numerical approach via the parabolic stability equation (PSE). Consequently, direct numerical simulation (DNS) has increasingly been elected as the preferred tool for investigating the complex interaction of flow and compliant surfaces.

The application of DNS to boundary layer compliant surface interaction is still very much in the preliminary stage. Current DNS studies are focused on simple homogeneous wall models to obtain results for validation against existing theoretical predictions. The early DNS works of Metcalfe et al. (1991) and Ehrenstein & Rossi (1996) employed a temporal model with periodic boundary conditions in the stream direction. The spatial evolution of disturbance waves was more recently studied by Davies & Carpenter (1997) (fully-developed channel flow), Wiplier & Ehrenstein (1997) and Wang et al. (2001) (boundary layer flow). Davis and Carpenter (2001) have also recently studied linear wave evolution in a 3D boundary layer over a rotating compliant surfaces.

In this paper, we shall report on the DNS work we have done on the spatial evolution of 2D linear waves in a Blasius boundary layer over finite-length viscoelastic layers, and 3D linear waves and nonlinear wave interaction in a Blasius boundary layer over finite membranes.

2D WAVE SIMULATIONS

The vorticity-streamfunction formulation was adopted for the study of the 2D waves. The finite difference scheme with variable-order accuracy was employed for spatial discretization. A fully implicit algorithm was used to deal with the fluid-structure problem. For 2-D incompressible perturbation flow field, the dimensionless governing equations can be written in vorticity-streamfunction form.

$$\frac{\partial\zeta}{\partial t}+\frac{\partial}{\partial x}(c_1\cdot u\zeta+c_2\cdot\bar{u}\zeta+c_2\cdot u\bar{\zeta})+\frac{\partial}{\partial y}(c_1\cdot v\zeta$$
$$+c_2\cdot\bar{v}\zeta+c_2\cdot v\bar{\zeta})=\frac{1}{\mathrm{Re}}(\frac{\partial^2\zeta}{\partial x^2}+\frac{\partial^2\zeta}{\partial y^2}) \quad (1)$$

$$\frac{\partial^2\psi}{\partial x^2}+\frac{\partial^2\psi}{\partial y^2}=\zeta \quad (2)$$

$$u=\frac{\partial\psi}{\partial y} \quad (3)$$

$$v=-\frac{\partial\psi}{\partial x} \quad (4)$$

where, ζ,ψ denote the perburbation vorticity and streamfunction fields respectively. $c_1 = 0$ and $c_2 = 1$, for linear perturbation of base flow $(\bar{u},\bar{v})$; $c_1 = 1$ and $c_2 = 1$, for nonlinear perturbation of base flow $(\bar{u},\bar{v})$; $c_1 = 1$ and $c_2 = 0$, for full Navier-Stokes equations.

In above equations, $\bar{u},\bar{v},\bar{\zeta}$ are the undisturbed base flow solutions of the flat plate boundary layer flow. Here, the Blasius similarity solution is used as the base flow. Re is the Reynolds number based on the free stream velocity of mean flow (U_∞*), the displacement thickness δ_0* at a suitable reference, and the kinematic viscosity (v*):

The material of the solid layer is assumed to be elast-dialatational and Voigt-deviatoric. Viscoelastic layers with finite thickness h and finite length is placed at $x_{cs} \le x \le x_{ce}$, $-h \le y \le 0$. Wave propagation in the layer obeys the following nondimensional dynamical equations:

$$\rho_s\frac{\partial^2\xi}{\partial t^2}=\frac{1}{2}(Y_{sr}+Y_{si}\frac{\partial}{\partial t})(\frac{\partial^2\xi}{\partial x^2}+\frac{\partial^2\xi}{\partial y^2})$$
$$+(\frac{Y_v}{3}+\frac{Y_{sr}}{6}+\frac{Y_{si}}{6}\frac{\partial}{\partial t})(\frac{\partial^2\xi}{\partial x^2}+\frac{\partial^2\eta}{\partial x\partial y}) \quad (5)$$

$$\rho_s\frac{\partial^2\eta}{\partial t^2}=\frac{1}{2}(Y_{sr}+Y_{si}\frac{\partial}{\partial t})(\frac{\partial^2\eta}{\partial x^2}+\frac{\partial^2\eta}{\partial y^2})$$
$$+(\frac{Y_v}{3}+\frac{Y_{sr}}{6}+\frac{Y_{si}}{6}\frac{\partial}{\partial t})(\frac{\partial^2\eta}{\partial y^2}+\frac{\partial^2\xi}{\partial x\partial y}) \quad (6)$$

Following Wang et al (2001), solid and fluid governing equations are nondimensionalized by the same reference length at the ribbon location. The viscoelastic layer investigated here possess the following nondimensional parameters: $\rho_{(L)}$=1.0, $Y_{sr(L)}$ =2.0, $Y_{si(L)}$ =0.0098, $Y_{\gamma(L)}$=150 where the wall reference Reynolds number $Re_{(L)}=2\times10^4$. Zero displacement boundary conditions are adopted on all the three sides of the compliant layer in contact with the rigid base. At the top surface of the viscoelastic layer, the stress boundary conditions are given,

$$\tau=\frac{Y_{sr}}{2}(\frac{\partial\xi}{\partial y}+\frac{\partial\eta}{\partial x})+\frac{Y_{si}}{2}\frac{\partial}{\partial t}(\frac{\partial\xi}{\partial y}+\frac{\partial\eta}{\partial x}) \quad (7)$$

$$\sigma=Y_{sr}\frac{\partial\eta}{\partial y}+Y_{si}\frac{\partial}{\partial t}(\frac{\partial\eta}{\partial y})+\frac{1}{3}(Y_v-Y_{sr})(\frac{\partial\xi}{\partial x}+\frac{\partial\eta}{\partial y})$$
$$-\frac{Y_{si}}{3}\frac{\partial}{\partial t}(\frac{\partial\xi}{\partial x}+\frac{\partial\eta}{\partial y}) \quad (8)$$

where the shear stress τ and normal stress σ are computed from the perturbation fluid velocity fields (u,v) and pressure field p_w at the mean flow-wall interface.

$$\tau=\frac{1}{\mathrm{Re}}(\frac{\partial u}{\partial y}+\frac{\partial v}{\partial x})_w \quad (9)$$

$$\sigma=-p_w+\frac{2}{\mathrm{Re}}(\frac{\partial v}{\partial y})_w \quad (10)$$

The perturbation pressure p_w at the wall can be derived by the vertical perturbation NS equation integrating from the free stream through the boundary layer to wall,

$$p_w=\int_{wall}^{freestream}(\frac{\partial v}{\partial t}+\frac{\partial(\bar{u}v+u\bar{v}+uv)}{\partial x}+\frac{\partial(2\bar{v}v+vv)}{\partial y}$$
$$-\frac{1}{\mathrm{Re}}(\frac{\partial^2 v}{\partial x^2}+\frac{\partial^2 v}{\partial y^2}))\cdot dy \quad (11)$$

The linear boundary conditions for the flow field over compliant surfaces are given as,

$$\zeta|_w=(\frac{\partial^2\psi}{\partial x^2}+\frac{\partial^2\psi}{\partial y^2})_w \quad (12)$$

$$\psi|_w=\int(-v_w)\,dx \quad (13)$$

$$\psi_y|_w=u_w \quad (14)$$

where u_w and v_w are the perturbation velocities at the wall, which are related to the displacement history of the compliant surface:

$$u_w=\begin{cases}0, & x<x_s \text{ or } x>x_e\\ \dfrac{\partial\xi}{\partial t}-\eta\dfrac{\partial\bar{u}}{\partial y}, & x_s\le x\le x_e\end{cases} \quad (15)$$

$$v_w=\begin{cases}0, & x<x_s \text{ or } x>x_e\\ \dfrac{\partial\eta}{\partial t}, & x_s\le x\le x_e\end{cases} \quad (16)$$

The fourth order accuracy central difference scheme at inner points and fourth order one sided difference scheme at boundary points are employed for spatial discretizations of solid governing equations. Uniform grid is employed for the solid layer. Three-point backward scheme is used for the temporal discretization of the wall equations.

The 2D waves in Blasius boundary layer over finite viscoelastic compliant layers were studied. Computational results showed that finite viscoelastic layers are able to reduce the amplification rates and the shrink the unstable region of TS waves (Fig.1). Wavenumber spectra also agree very well with eigenvaules predicted by linear stability theory (Yeo 1988). Therefore, the results are in reasonably agreement with predictions of linear stability theory (infinite-length). Fig. 2 shows the deformation of a viscoelastic layer associated with the passage of a wave.

3D WAVE SIMULATIONS

The fractional step method for coupling 3D perturbation Navier-Stokes equations and deformable membrane equation is developed and described in this section. Using this method, 3D linear wave and wave interactions inside transitional boundary layer over compliant surfaces are simulated.

3D Computational Algorithm

The 3D incompressible perturbation flow field is governed by the perturbation continuity and the Navier-Stokes equations:

$$\frac{\partial u_i}{\partial x^l} = 0 \tag{17}$$

$$\frac{\partial u_k}{\partial t} + \frac{\partial}{\partial x^l}(c_2 \cdot \overline{u_l} u_k + c_2 \cdot \overline{u_k} u_l + c_1 \cdot u_l u_k) = \frac{\partial}{\partial x^l}(\frac{1}{\mathrm{Re}} \frac{\partial u_k}{\partial x^l}) - \frac{\partial p}{\partial x^k} \tag{18}$$

Once again, $c_1 = 0$ and $c_2 = 1$, for linear perturbation of the Navier-Stokes equations; $c_1 = 1$ and $c_2 = 1$, for nonlinear perturbation of the Navier-Stokes equations; $c_1 = 1$ and $c_2 = 0$, for the full Navier-Stokes equations. In above equations, Re is the Reynolds number based on the free stream velocity of mean flow (U_∞), the displacement thickness (δ_{x0}) at the location where the ribbon is placed, and the kinematic viscosity (ν). x^1, x^2 and x^3 indicate the streamwise (x), wall normal (y) and spanwise (z) directions, respectively. The velocity component u_1, u_2 and u_3 in the x-, y- and z- directions are used interchangeably with u, v and w. The subscript w denotes the value at the wall. u and $\overline{u}$ indicate the perturbation and base flow velocity components respectively.

The finite volume method is adopted for spatially discretizing perturbation Navier-Stokes equations on a non-staggered grid system. Three steps fully implicit fractional step method is developed for solving perturbation flow field. In our work, pressure correction algorithm is employed. First of all, momentum equations are integrated based on pressure field at previous time step:

$$\frac{3u_k^* - 4u_k^m + u_k^{m-1}}{2\Delta t} + \frac{\partial}{\partial x^l}(c_2 \cdot \overline{u_l} u_k^* + c_2 \cdot \overline{u_k} u_l^* + c_1 \cdot u_k^* u_l^*) = \frac{\partial}{\partial x^l}(\frac{1}{\mathrm{Re}} \frac{\partial u_k^*}{\partial x^l}) - \frac{\partial p^m}{\partial x^k} \tag{19}$$

Thereafter, corrective pressure field is solved based on the intermediate velocity field,

$$\frac{\partial}{\partial x^k}\frac{\partial \pi}{\partial x^k} = \frac{3}{2\Delta t}\frac{\partial u_k^*}{\partial x^k} \tag{20}$$

Thereafter, velocity and pressure fields are updated using,

$$u_k^{m+1} = u_k^* - \frac{2\Delta t}{3}\frac{\partial \pi}{\partial x^k} \tag{21}$$

$$p^{m+1} = p^m + \pi \tag{22}$$

To fully couple the perturbation flow field and solid equations, several inner iterations are needed.

The spring-backed isotropic tensioned membrane with foundation and damping is used in this study. The nondimensional governing equation of this compliant surface is,

$$m\frac{\partial^2 \eta}{\partial t^2} + d\frac{\partial \eta}{\partial t} - T(\frac{\partial^2 \eta}{\partial x^2} + \frac{\partial^2 \eta}{\partial z^2}) + k\eta = -p_w \tag{23}$$

The finite membrane spans (x_{cs}, x_{ce}) in the streamwise direction. Hence at the two ends of the membrane,

$$\eta(x_{cs}) = \eta(x_{ce}) = 0 \tag{24}$$

Periodic boundary condition is specified in the spanwise direction for consistency with the periodic character of the perturbation in spanwise direction. The perturbative fluid velocity (u_w,v_w,w_w) at the wall is coupled with the displacement of the surface by,

$$u_w = \begin{cases} 0, & x \le x_s \text{ or } x \ge x_e \\ -\eta\dfrac{\partial \overline{u}}{\partial y}, & x_s < x < x_e \end{cases} \tag{25}$$

$$v_w = \begin{cases} 0, & x \le x_s \text{ or } x \ge x_e \\ \dfrac{\partial \eta}{\partial t}, & x_s < x < x_e \end{cases} \quad (26)$$

$$w_w = 0 \quad (27)$$

The three points backward Euler difference scheme is used to temporally discretize fluid membrane governing equation. The fourth order accuracy central difference scheme is employed for spatial discretizations of solid governing equations.

3D Oblique waves

The simulation of 3D oblique TS waves over a finite membrane is performed. Membrane parameters are set to $Re_{(L)}$=580, $m_{(L)}$=1.0, $T_{(L)}$=10, $d_{(L)}$=0.1, $k_{(L)}$=0. The compliant membrane is placed between Re_{cs}= 941.94 and Re_{ce}=1236.04. These CIFI waves excited by the same frequency and the same spanwise wavenumber usually possess a different streamwise wavenumber and therefore travel at a different angle compared with the TS wave. Superposition of these waves causes crests of original oblique TS wave to deviate from a straight line. (Fig. 3). The same phenomenon is more clearly seen for a compliant surface (Fig. 4) as the amplitudes of the CIFI wave is generally larger at the compliant surface.

Subhamonic Breakdown

The earlier transitional behavior of Blasius boundary layer over a finite membrane is simulated and presented in this section. The finite membrane ($m_{(L)}$=12.0, $T_{(L)}$=6.96, $d_{(L)}$=0., $k_{(L)}$=0. and $Re_{(L)}$=661.) employed in our simulation of nonlinear breakdown is selected from Metcalfe et al (1990). The linear boundary conditions were also employed in their temporal DNS of transitional boundary layer over finite panel.

The comparison of perturbation velocity u contour at t=8T for rigid wall and compliant membrane are presented. It is observed that the Λ vortices over finite membrane are much more sharper compared to the counterpart over rigid wall (Fig. 5). Due to the longer wavelength of the 2D TSI, the streamwise spacing of the Λ vortices is longer for the membrane. Furthemore, the nonlinear breakdown over finite membrane is obviously less intense compared to the latter. This could be caused by: 1) reduced amplification rate of 2D and 3D TS waves over the memebrane surface; 2) increased propagation angle of 3D oblique TS wave and the weaker nonlinear interactions.

Fundamental breakdown

In this simulation, membrane parameters are the same as those used in the subharmonic breakdown above. The comparison of perturbation velocity u contour at t=8T for rigid wall and compliant membrane is presented in Fig 6, with corresponding surface deformation given in Fig 7. The perturbation appears to be more intense for the membrane case

The flooded contours of the total velocity $u+\bar{u}$ at 'peak location' for rigid wall and finite membrane (z=0, t=8T) is presented in Fig 8a-b. Nonlinear breakdown seems to occur earlier for membrane surface. This fact seems to be in constrast with Metcalfe et al (1990)'s results, which conclude that compliant membrane generally lessen the intensity of nonlinear perturbation. However, the comparison conducted in this study may not be 'fair' for compliant surface. Based on our experiences for simulating fundamental breakdown over rigid wall, we learn that the onset location of 'first spike' is affected by the amplitude of perturbations. We also know that 2D as well as 3D TS waves excited by the same outside excitation may possess higher amplitude over compliant surfaces than over a rigid wall due to the Hooke's law. This additional amplification effect of compliant surfaces may cause the amplitudes of perturbation waves reach the threshold value earlier over compliant surfaces than over a rigid wall and could be the reason for the 'earlier fundamental breakdown' over compliant membrane observed in current study. Therefore, such a negative side effect of compliant surface may not be so harmful in linear stage (unless the wall is very soft), but may be quite dangerous during the stage of 'spike formation'.

REFERENCE

Carpenter P.W. and Garrad A.D., 1985, "The hydrodynamics stability of flow over Kramer-type compliant surfaces. Part1 Tollmien-Schliching instabilities", *Journal of Fluid Mechanics*, vol. 155, p.465.

Carpenter P.W. and Garrad A.D., 1986, "The hydrodynamics stability of flow over Kramer-type compliant surfaces. Part2 Flow induced surface instabilities", *Journal of Fluid Mechanics*, vol. 170, p.199.

Davies C. and Carpenter P.W., 1997, "Numerical simulation of the evolution of Tollmien-Schlichting waves over finite compliant panels", *Journal of Fluid Mechanics*, vol.335, p.361.

Davis C. and Carpenter P.W., 2001, "A Novel velocity-vorticity formulation of the Navier-Stokes equations with applications to boundary layer disturbance evolution", *Journal of Computational Physics* vol.172, p.119.

Domaradzki J.A. and Metcalfe R.W., 1987, "Stabilization of laminar bounary layers by compliant membranes", *Physics of Fluids*, vol.30 (3), p.695.

Ehrenstein U. and Rossi M., 1996 "Nonlinear Tollmien-Schlichting waves for a Blasius flow over compiant coatings", *Physics of Fluids*, vol.8 (4), p.1036.

Fasel H. and Kozelmann U., 1990, "Nonparallel stability of a flat-plate boundary layer using the compelete Navier-Stokes equations", *Journal of Fluid Mechanics*, vol.221, p.311.

Liu C. and Liu Z., 1995, "Multigrid mapping box relaxation for simulation of the whole process of flow transition in 3D boundary layer", *Journal of Computational Physics*, vol.119:(2), p.325.

Metcalfe R.W., Battistoni F., Orzo S. and Ekeroot J., 1991, "Evolution of boundary layer flow over a compliant wall during transition to turbulence", *Proceedings of Royal Aeronautical Society*, p.36.1

Thomas M.D., 1992a, "On the resonant triad interaction in flows over rigid and flexible boundaries", *Journal of Fluid Mechanics*, vol. 234, p.447.

Thomas M.D., 1992b, "The nonlinear stability of flows over compliant walls", *Journal of Fluid Mechanics*, vol. 239, p.657.

Wang Z., Yeo K.S. and Khoo B.C., 2001, "Numerical simulation of 2D Tollmien-Schlichting waves over finite membrane", *Proceedings of 9th Annual Conference of the CFD Society of Canada*, p453.

Wiplier O. and Ehrensein U., 2000, "Numerical simulation of linear and nonlinear Disturbance evolution in a boundary layer with complaint walls", *Journal of Fluid and Structures*, vol.14, 2000, p.157.

Yeo K.S., 1986, "The stability of flow over flexible surfaces", *Ph.D. Thesis*, University of Cambridge.

Yeo K.S., 1988, "The stability of boundary-layer flow over single- and multi-layer viscoelastic walls", *Journal of Fluid Mechanics*, vol. 196, p.359.

FIGURES

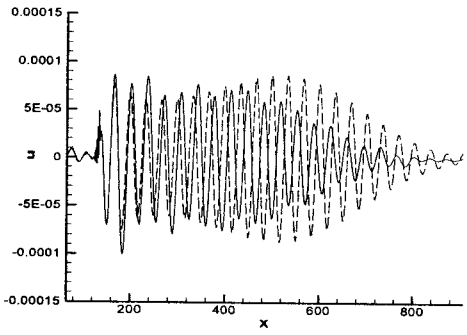

(a)

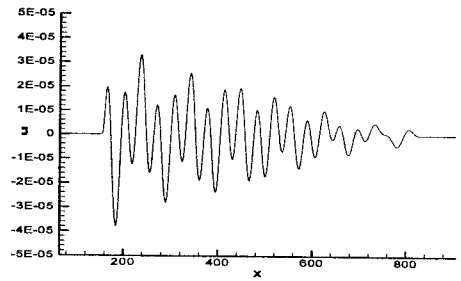

(b)

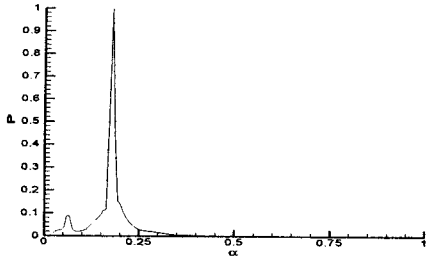

(c)

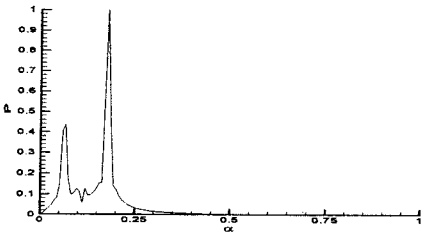

(d)

Fig 1. Computational results for 2D unsteady boundary layer over volume-based wall. (a)Comparison of velocity u distribution in a boundary layer over a viscoelastic layer (solid line) and rigid wall (dashed line) at y=1.05. (b) velocity u at wall. (c)Wavenumber spectrum for velocity u at y=1.05 (Solid line for viscoelastic layer, dashed line for rigid wall). (d) Wavenumber spectrum for velocity u at wall (volume-based wall).

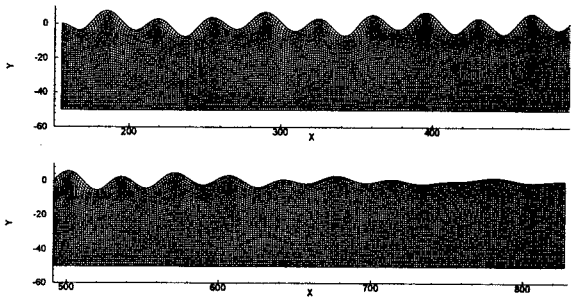

Fig.2. Defomation of solid layer (scale factor 100,000)

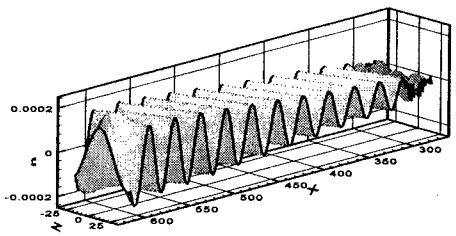

(a)

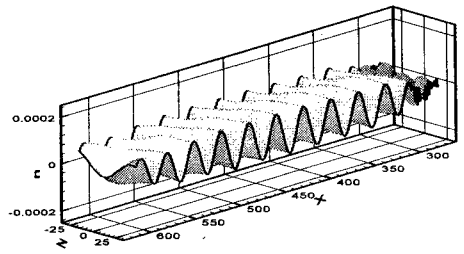

(b)

Fig 3. Comparisons of perturbation velocity u at y=0.56. (a) 3D oblique wave over rigid wall, (b) 3D oblique wave over finite membrane

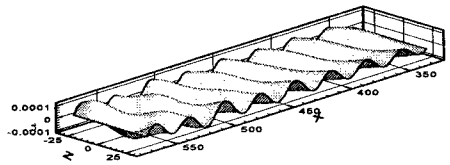

(a)

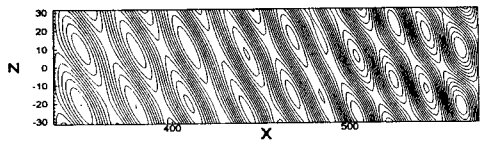

(b)

Fig 4. Membrane displacement (a) displacement distribution (b) contour of membrane displacement

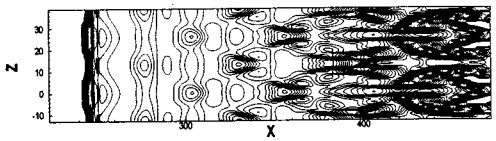

(a)

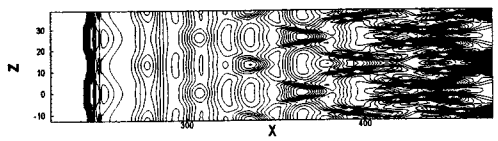

(b)

Fig 5. Comparison of perturbation velocity u contour at (t=8T) for rigid wall (a) and compliant surfaces (b) during subharmonic breakdown.

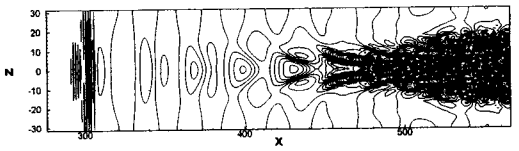

(a)

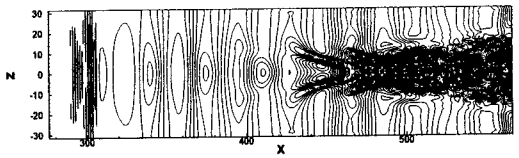

(b)

Fig 6. Comparison of perturbation velocity u contour at (t=8T) for rigid wall (a) and compliant surfaces, (b) during fundamental breakdown.

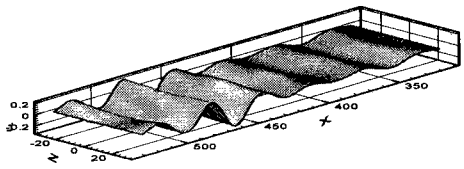

Fig 7. Membrane displacement during fundamental breakdown (t=8T).

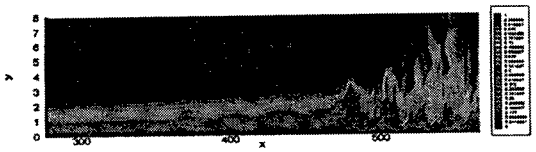

(a)

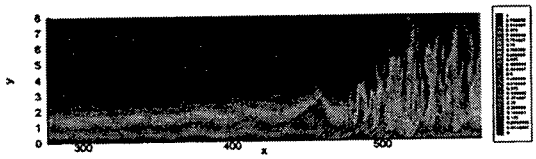

(b)

Fig 8. Comparison of total velocity $u+\bar{u}$ countour (flood based) at z=0, t=8T during fundamental breakdown. (a) rigid wall, (b) finite membrane.